

A decade-long hydrographic moored time series near the Drygalski Ice Tongue, Terra Nova Bay, Ross Sea.

Liv Cornelissen^{1,2}, Sukyoung Yun³, Jasmin McInerney¹, Brett Grant¹, Fiona Elliott^{1,5},
Seung-Tae Yoon^{3,4}, Christopher J Zappa⁶, Won Sang Lee³, and Craig Stevens^{1,2}

¹Earth Sciences New Zealand, formerly National Institute of Water and Atmospheric Research, Greta Point, Wellington 6021, New Zealand

²Department of Physics, University of Auckland, Auckland 1142, New Zealand

³Korea Polar Research Institute, Yeosu-gu, Incheon 21990, Republic of Korea

⁴now at Kyungpook National University, Daegu, South Korea

⁵now at University of Bergen, Norway

⁶Lamont Doherty Earth Observatory, Columbia University, Palisades, NY, USA

Correspondence: Liv Cornelissen (liv.cornelissen@niwa.co.nz)

Abstract. In this paper we describe a decade-long timeseries of hydrographic mooring observations adjacent to the Drygalski Ice Tongue in southern Terra Nova Bay, Antarctica. Unique aspects of the data are that (i) the instruments were placed very close to the Ice Tongue which has significant influence on the region's ocean and sea ice, and (ii) the upper sensors were positioned relatively close (< 100 m) to the ocean surface compared to typical Antarctic moorings. Starting in December 2014, the mooring array included three locations - the Drygalski Basin, the edge of the Crary Bank and, on the southern side of the ice tongue, in Geikie Inlet. The instruments measure temperature, salinity, pressure, and current velocity. The "DITx" mooring locations were chosen in order to support questions regarding the influence of the Drygalski Ice Tongue on regional ocean processes. The observations are relevant to water mass formation, glaciology and ice melt, sea ice production and decay, ice shelf cavity processes - as well as regional marine ecosystem processes. The data from the instruments show the seasonal cycle along with interannual variability, as well as a range of singular events. All data can be downloaded from the SEANOE database.

Copyright statement. CC-BY

1 Introduction

1.1 The Drygalski Ice Tongue and Terra Nova Bay

The Drygalski Ice Tongue is presently the largest ice tongue in Antarctica and it forms the southern boundary of Terra Nova Bay (TNB), Western Ross Sea, Antarctica. It is the floating extension of the David Glacier and plays a crucial role in main-

20 taining the Terra Nova Bay polynya by limiting northward-flowing of sea ice along the Victoria Land Coast (Gomez et al., 2023). The free floating part of the ice tongue extends ~ 80 -90 km into the Ross Sea, with a width of ~ 20 km (Stevens et al., 2017) as shown in Figure 1, which makes it presently Antarctica's largest free-floating glacier (Frezzotti & Mabin, 1994). At the grounding line the glacier is more than 1900 m thick (Indrigo et al., 2021; Bianchi et al., 2001). The glacier then thins to the extent that the tip, located above the edge of the Crary Bank in a water depth of 600-700 m, is ~ 200 m thick (Indrigo et al., 2021). Despite the blocking effect of the ice tongue on sea ice and surface water masses, Stevens et al. (2024) determined that there is exchange and advection of water masses in the ocean below the floating ice.

25

Terra Nova Bay is bounded to the south by the Drygalski Ice Tongue and to the west by the Nansen Ice Shelf, which is fed by the Priestly and Reeves Glacier. A key bathymetric feature, the Drygalski Basin, extends north east into the Drygalski Trough and is believed to be the primary export pathway for High Salinity Shelf Water (HSSW). Along the eastern boundary, the Victoria Land Coast Current carries water and sea ice northward from McMurdo Sound (Stevens et al., 2017). This flow has 30 been inferred from satellite sea ice drift and surface drifters (Greg Leonard, Antarctic Science Platform's Sea Ice and Carbon Cycle Feedbacks Project) and is reproduced in ocean circulation models such as GLORYS and P-SKRIPS (Malyarenko et al., 2023; Gossart et al., pre-print), though its vertical structure and depth extent remain poorly constrained by direct observations between McMurdo Sound and Terra Nova Bay. This current could also bring water masses into Terra Nova Bay below the Drygalski Ice Tongue or along the Drygalski Ice Tongue as replenishing the HSSW outflow.

35

The polynya that occasionally forms in Terra Nova Bay is relatively small in extent when compared to the nearby Ross Sea polynya (Maqueda et al., 2004) but plays an important role in the global climate system. Between autumn and spring, strong katabatic winds blow off the Nansen Ice Shelf, pushing the sea ice off the coast and enabling heat loss from the relatively warm ocean to the cold atmosphere, and producing sea ice and HSSW. Despite its small size in global terms, Terra Nova Bay 40 accounts for approximately 3–4% of Antarctic sea ice production (Tamura et al., 2016), and up to 10% of Antarctic Bottom Water (AABW). Sea ice makes ship-based observations very difficult from late autumn when these important water masses are formed and HSSW is an important water mass that contributes to basal melting of floating glaciers and ice shelves (Nicholls, 1997). Hydrographic moorings, that observe water masses throughout the year are therefore an essential tool to study the oceanographic processes in Terra Nova Bay polynya. While moorings in the central Terra Nova Bay have provided a long term 45 perspective of water mass transformation (MORSea: Marine Observatory in the Ross Sea, 2009; Castagno et al., 2019), the strong influence of the Drygalski Ice Tongue on the region provided motivation for a mooring array (hereinafter called the "DITx" array) focused around the Drygalski Ice Tongue.

1.2 Processes that interact with the Drygalski Ice Tongue

50 One of the key processes influencing the region are the occasional katabatic-driven polynya events. In such conditions, the fast, cold katabatic winds drive sea ice formation at the ocean surface, which results in the creation of HSSW as a by-product (e.g.,

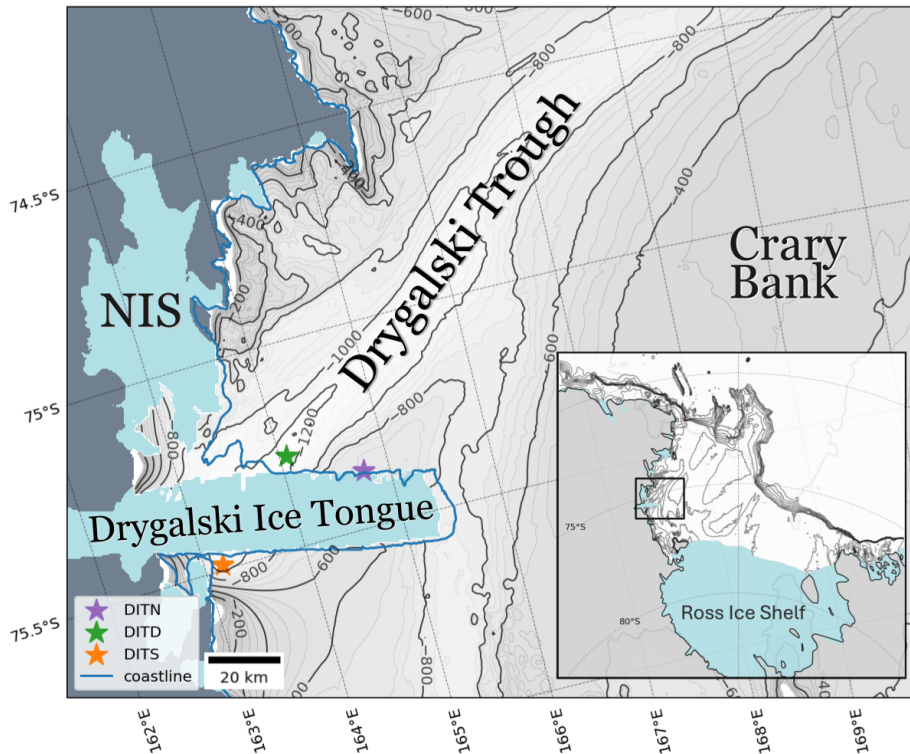


Figure 1. Terra Nova Bay (TNB) is located in the western Ross Sea. The Nansen Ice Shelf (NIS) bounds the bay in the west, the Drygalski Ice Tongue bounds the bay on the southern side and the deepest part of Terra Nova Bay is the Drygalski Basin. The eastern boundary of the Drygalski trough is the Crary bank. The DITx mooring locations are marked on the bathymetry of Terra Nova Bay with a Star, the grey contours are the bathymetry at 50 m intervals with solid lines on 200 m intervals. The light-blue area represents the floating sea ice, the Nansen Ice shelf and Drygalski Ice Tongue. The grey represents the land. DITN mooring was first deployed in December 2014, DITD was first deployed in February 2017 and DITS was deployed from February 2017 until January 2020.

Yoon et al., 2020; Friedrichs et al., 2022). The brine rejection from the sea ice formation first breaks down the stratification of the water column in the polynya before HSSW starts to form. While the production of HSSW begins in late Autumn/ early winter, the salinity increase does not increase until September at the bottom in the eastern side of Terra Nova Bay, where DITN is located, and in the Drygalski Basin (Yoon et al., 2020). Figure 2 shows the seasonal evolution of stratification in Terra Nova Bay, based on a summer CTD profile and Argo float observations from both summer and winter (Argo, 2000). The circulation pattern in Terra Nova Bay is described by Yoon et al. (2020), based on summer CTD observations and three hydrographic moorings between December 2014 and March 2018 and include data from the hydrographic moorings described in this paper (DITN and DITD). They observed a cyclonic circulation in the deeper part of Terra Nova Bay between 400-700 m during the summer, which advects the HSSW created close to the Nansen Ice shelf, which is considered to be the primary location of HSSW production in Terra Nova Bay, towards the DITN, where the salinity increase is observed by the bottom instrument of

this mooring. The salinity increases at this depth are observed between September and October, and not at the start of winter when the stratification has broken down. Rusciano et al. (2013) suggested that HSSW is advected from the Nansen Ice Shelf front towards eastern Terra Nova Bay and was confirmed in Yoon et al. (2020).

65

Terra Nova Bay Ice Shelf Water (TISW) is formed when HSSW interacts with basal melt waters from the Drygalski Ice Tongue and the Nansen Ice Shelf during active HSSW production. TISW is characterized by a conserved temperature below the surface freezing temperature around -1.94°C depending on the salinity (Yoon et al., 2020) and a density larger than 1028 kg/m^3 (e.g., Rusciano et al., 2013; Yoon et al., 2020), [fig 6 in (Yoon et al., 2020)]. The characteristics of TISW observed in summer in
70 Yoon et al. (2020) depends on observation period and the outflow from under the Nansen Ice Shelf and is believed to advect in the same cyclonic circulation as HSSW towards the eastern Terra Nova Bay. TISW is also observed in the eastern Terra Nova Bay close to Drygalski Ice Tongue by DITN; further study needs to investigate if this TISW is formed under the Nansen Ice Shelf and advected or is formed when HSSW interacts with basal melt waters from the Drygalski Ice Tongue itself. Antarctic Surface Water (AASW) can be found at the subsurface and originates from the melting of the sea ice. It is a fresh and relatively
75 warm ($>-1.7^{\circ}\text{C}$, (Friedrichs et al., 2022)) water mass as it warms through solar radiation during Summer (Rusciano et al., 2013). As its density is much lower than the water masses formed during winter, it contributes to the restratification of the water column during the summer months. The stratification driven by the AASW and the breakdown of the stratification driven by the HSSW formation is shown in Figure 2. The CTD profiles are also used for instrument calibration, as described in *section 2.1* and Figure 2.

80

1.3 Monitoring the water masses around the Drygalski Ice Tongue

The DITx hydrographic moorings distributed around the Drygalski Ice Tongue have been maintained since December 2014 in order to monitor the water mass properties and currents close to the ice tongue. Three moorings were deployed over different time frames, located around the Drygalski Ice Tongue as shown in Fig. 1. DITN is a long mooring deployed on the northern
85 side of the Drygalski Ice Tongue from December 2014 to the present. It includes instruments near the seafloor, mid-water column, and subsurface, with the shallowest instrument at 75 m depth. The upper instruments are at risk of collisions from icebergs calving off the Drygalski Ice Tongue, which are frequent in the area and can extend to great depths. Despite this risk, the setup is unique and essential for studying subsurface processes. Its proximity to the ice tongue and near-surface coverage make it particularly well suited to investigate subsurface circulation and the influence of meltwater. DITD, a short mooring
90 deployed in February 2017 and still active, is located in the deepest part of the Drygalski Basin. It captures the densest HSSW observed in the area, offering a valuable reference point for comparing water mass properties with other locations. DITS was a long mooring positioned south of the Drygalski Ice Tongue in Geikie Inlet and was maintained from February 2017 until January 2020. This paper presents a comprehensive overview of the decadal dataset collected by the DITx array. The data are freely available via SEANOE in netCDF format, organized by mooring, instrument type, and deployment year (Cornelissen

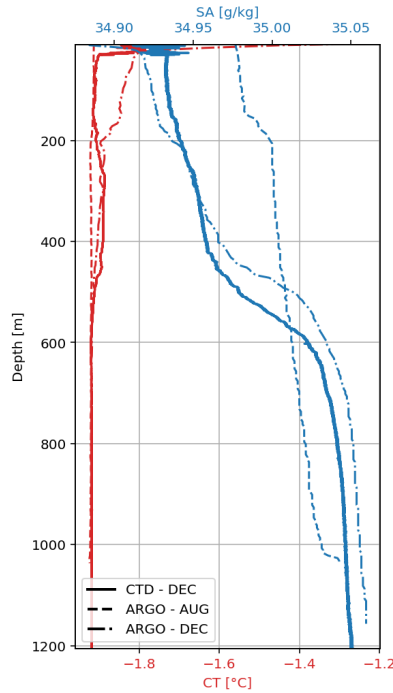


Figure 2. Vertical profiles of conservative temperature (red) and absolute salinity (blue) within Terra Nova Bay. The CTD profile from December 2022 is shown as solid lines, while ARGO float ((Argo, 2000)) measurements are shown for winter (dashed lines) and summer (dash-dotted lines). This comparison highlights seasonal variations in the upper water column.

95 et al., 2025). Tables 3, 4, and 5 summarize the mooring configurations, and instrument placements are visualized in Fig. 3 and 4.

In addition to these moorings, other relevant datasets in the region include the MORSea Moorings D and L (MORSea: Marine Observatory in the Ross Sea, 2009; Castagno et al., 2019) and a Lamont-Doherty Earth Observatory (LDEO) mooring (Miller et al., 2024) located near the front of the Nansen Ice Shelf (Miller et al., 2024). Since 2013, Argo floats have also contributed
 100 valuable data to the Ross Sea, with four deployed in Terra Nova Bay during 2021, 2022, 2024, and 2025 (Argo, 2000).

2 The DITx hydrographic mooring time series

Three hydrographic moorings have been deployed from December 2014 in the Terra Nova Bay polynya equipped with CTD instruments (Sea-Bird Scientific SBE37SM and SBE37SMP, Bellevue), thermistors (Sea-Bird Scientific SBE56, Bellevue) and current meters (RCM9 (Xylem. Inc., Rye Brook) until 2017 and Aquadopp (Nortek, Norway) from 2017. The accuracy of the
 105 instruments are shown in Table 1 for the temperature and salinity and Table 2 for the current velocity. Measurement uncertainty is represented as shaded bands in the figures and is based on the manufacturer-specified initial accuracy for each instrument and measured variable.

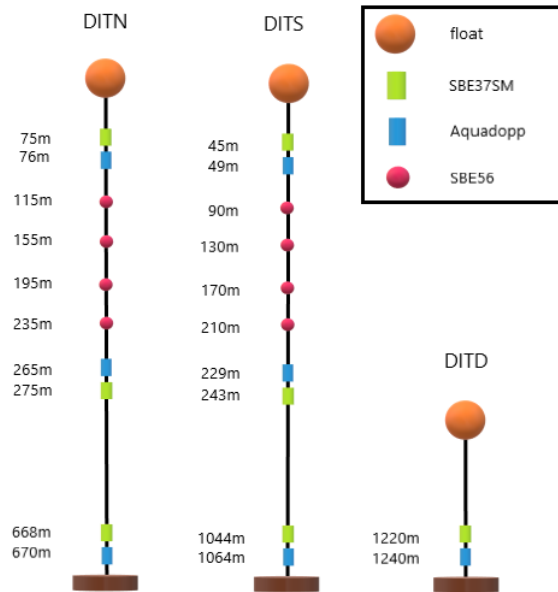


Figure 3. A schematic figure of the set up of the three moorings deployed around the Drygalski Ice Tongue in Terra Nova Bay. The DITN has been deployed since December 2014 until present, the DITS between February 2017 and January 2020 and the DITD from February 2017 until present. The Long moorings DITN and DITN have three pairs for CTD (SBE37SMP/SBE37SM) and current meters (Aquadopp) and an sequence of 4 thermistors (SBE56). Floats are indicative, see Figure A1 for full schematic mooring diagram.

Instrument	Measurement range	Initial Accuracy
SBE37SM	-5 to + 35°C	0.002°C
Aquadopp	-4 to + 40°C	0.1°C
SBE56	-5 to + 45°C	0.002°C
RCM9	-3.01 to + 5.92°C	0.05°C
SBE37SM	0-7 S/m 0-42 PSU	0.0003 S/m 0.003 - 0.01 PSU

Table 1. The accuracy of the Thermo-haline instruments based on their manuals. The accuracy of the salinity is not given directly as it is calculated with the conductivity and temperature and the accuracy has been determined by lab experiments (Sea-Bird Scientific , n.d.).

Instrument	Velocity range	Initial Accuracy	Magnetic resolution
Aquadopp	± 100 cm/s, ± 250 cm/s, ± 500 cm/s	$\pm 1\%$ of measured value ± 0.5 cm/s	2° for tilt < 30°
RCM9	0 to 300 cm/s	0.3 cm/s	5° for 0-15° tilt

Table 2. The accuracy of the hydrodynamic instruments based on their manuals. The accuracy of the salinity is not given directly as it is calculated with the conductivity and temperature.

110 The Drygalski Ice Tongue North mooring (DITN) is located on the northern side of the Drygalski Ice Tongue close to the ice tongue and was first deployed in December 2014. The bottom anchor sits at ~ 690 m depth. The DITN contains 4 groups of instruments, at the subsurface at ~ 75 m depth a MicroCAT SBE37SM and an Aquadopp/RCM9, between 115 m - 235 m depth. 4 SBE 56 thermistors, each 40 m vertical meters apart, a MicroCAT SBE37SM and Aquadopp/RCM9 at ~ 275 m depth and a MicroCAT SBE37 and Aquadopp/RCM9 close to the bottom at ~ 670 m depth. The RCM9 was used on the moorings: 1412DITN, 1512DITN and 1702DITN, the Aquadopp was first used on mooring 1702DITN, 1702DITD and 1702DITS and all future moorings.

115

The Drygalski Ice Tongue Deep mooring (DITD) is located slightly north-west of the DITN, in the Drygalski Basin anchored at ~ 1250 m depth. This mooring is equipped with 2 instruments near the bottom, a MicroCAT SBE37 and an Aquadopp at around 1240m depth. In 2018, there were 2 mooring groups, both containing a MicroCAT SBE37 and an Aquadopp, at ~ 1140 m and ~ 1240 m depth.

120

The Drygalski Ice Tongue South mooring (DITS) was deployed on the southern side of the Drygalski Ice Tongue between February 2017 until January 2020. In the first deployment year between February 2017 and March 2018, it was equipped with a MicroCAT SBE37SM and an RCM9 at ~ 190 m depth, 4 thermistors between 230 m and 250 m each 40 m apart, a MicroCAT SBE37SM and an RCM9 at ~ 400 m depth and a MicroCAT SBE37SM and an RCM9 at ~ 1100 m depth. The second deployment was equipped with three MicroCAT SBE37SM and an Aquadopp pairs at ~ 48 m depth, at ~ 230 m depth and at ~ 1050 m depth and 4 thermistors between 90 m and 210 m, spaced 40 m apart.

125

Each mooring was retrieved and redeployed every 1 to 2 years on a voyage, where the data is downloaded and instruments are serviced, battered, checked and calibrated before being deployed again. The MicroCAT SBE37SM(P) measures temperature, salinity (through conductivity) and pressure, the Aquadopp measures temperature, pressure, the direction and speed of the current and heading, pitch and roll, the SBE56 measures the temperature and RCM9 measures the speed and direction of the current. The depth averages described here is the mean depth derived from the pressure. The depth in each file in SEANOE is the mean depth derived from the pressure during that deployment. Outliers from mooring motions did not affect the mean significantly as the mean and median taken from the time-varying pressure are within the same depth in m.

135

2.1 Quality control

A number of checks are carried out to provide some assurance on data quality. The data collected by the instruments of the moorings are combined into netcdf files for each of the moorings per instrument type and deployment year. An overview of the available data is summarized in Table 3, 4 and 5. The data is also checked on faulty and missing data, which are described in the corresponding section in the '*Data overview*' section. In some cases, the instruments started the measurement timeseries whilst still on the ship, this resulted in $+20^\circ$ temperatures, and pressure measurements at sea level. This data is removed in

140

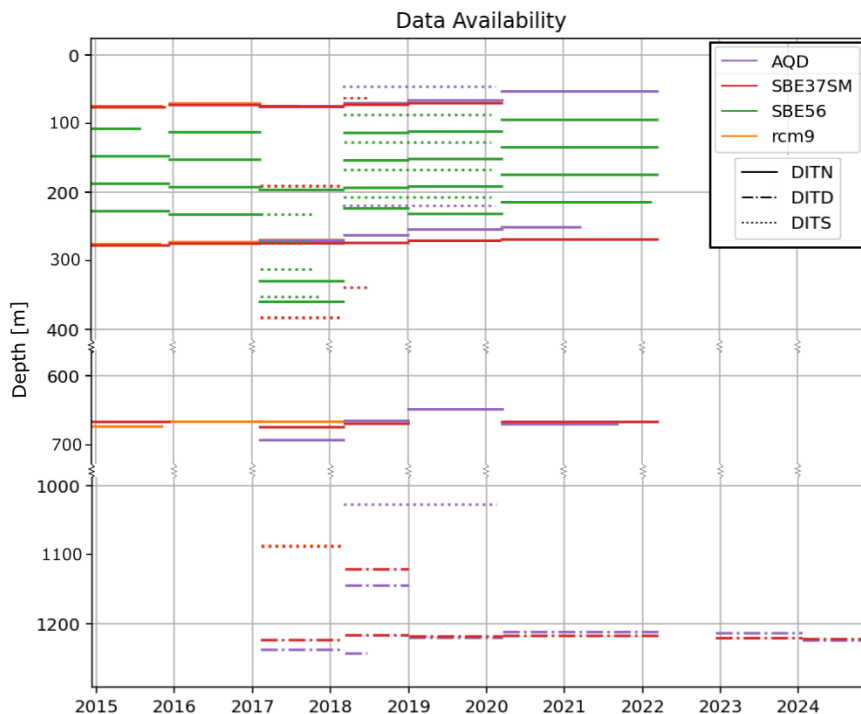


Figure 4. The data availability for each of the instruments at their corresponding depth based on the pressure measurements. The solid line are the instruments on the DITN, the dotted line on the DITD and the dot-dashed line on the DITS. The colors correspond with the instrument type, purple for the Aquadopp, red for the ctd SBE37SM(P), green for the thermistor SBE56 and orange for the current meter RCM9.

before the data processing.

The SBE37SM(P) instruments are calibrated before deployment by the CSIRO Oceanographic Calibration Facility to a factory calibration. The salinity is calculated through the conductivity and temperature. The accuracy of the salinity measurements have been examined by Uchida et al. (2008). The initial accuracy is found to be 0.003 PSU, or in TNB 0.0030 g/kg. Across different CTD instruments from Seabird, during long-term deployments (>1 year) accuracy drifts to 0.01 PSU (0.01008 g/kg in TNB) in regions of strong temperature gradients (Wong et al., 2023). These uncertainties are below the range of seasonal and interannual variability and the instrument errors are solely in the range of the winter conditions and these instruments are very stable (Sea-Bird Scientific, n.d.). The variability during winter is still valuable information as the instrument errors are a shift, rather than noise. In addition to the factory calibration, a full-depth CTD cast was conducted right after each mooring deployment and again prior to recovery to use for the instrument drift calibration. The CTD profiles were obtained within a few hundred meters of the mooring location, as close to the mooring site as the environmental condition allowed, with a safety buffer to avoid entanglement with the mooring lines. The salinity measurements of the moored SBE37SM(P) instruments are

Instrument	Location	Depth [m]	Type	sn	start [d/mm/yr]	end [d/mm/yr]	interval [s]	data quality	
DITN - 1412	75 21.612 S, 164 44.971 E	75	RCM9	647	12/12/2014	20/11/2015	1800	No T data,	
		77	SBE37SM	5675	12/12/2014	20/11/2015	600		
		108	SBE56	2086	12/12/2014	27/7/2015	30		
		148	SBE56	2088	12/12/2014	10/12/2015	30		
		188	SBE56	2089	12/12/2014	10/12/2015	30		
		228	SBE56	2090	12/12/2014	10/12/2015	30		
		276	RCM9	845	12/12/2014	30/10/2015	1800		
		278	SBE37SM	7284	12/12/2014	10/12/2015	600		
		667	SBE37SM	5838	12/12/2014	10/12/2015	600		
		674	RCM9	847	12/12/2014	6/11/2015	1800		No T data,
DITN - 1512	75 21.605 S, 164 44.918 E	71	RCM9	647	14/12/2015	8/2/2017	3600	T data faulty, removed	
		73	SBE37SM	5675	14/12/2015	8/2/2017	600		
		113	SBE56	5487	14/12/2015	8/2/2017	30		
		153	SBE56	2088	14/12/2015	8/2/2017	30		
		193	SBE56	2089	14/12/2015	8/2/2017	3S		
		233	SBE56	2090	14/12/2015	8/2/2017	30		
		273	RCM9	845	14/12/2015	8/2/2017	3600		
		275	SBE37SM	7284	14/12/2015	8/2/2017	600		
		666	SBE37SM	5838	14/12/2015	8/2/2017	600		No P recorded
		667	RCM9	847	14/12/2015	8/2/2017	3600		No T data
DITN - 1702	75 21.646S 164 44.788E	75	RCM9	1256	9/2/2017	1/8/2017	3600		
		75	SBE37SM	15239	9/2/2017	6/3/2018	120		
		76	AQD	13050	9/2/2017	6/3/2018	900		
		197	SBE56	4673	9/2/2017	6/3/2018	10		
		270	RCM9	1259	9/2/2017	6/3/2018	3600		
		271	AQD	9929	9/2/2017	6/3/2018	900		
		275	SBE37SM	15240	9/2/2017	6/3/2018	120		
		330	SBE56	4852	9/2/2017	6/3/2018	10		
		360	SBE56	4854	9/2/2017	6/3/2018	10		
		667	RCM9	342	9/2/2017	6/3/2018	3600		
		675	SBE37SM	15257	9/2/2017	6/3/2018	120		
		694	AQD	9930	9/2/2017	6/3/2018	900		

155 post-calibrated with the profile measurements using the depth of the moored instruments.

Instrument	Location	Depth [m]	Type	sn	start	end	interval [s]	data quality	
DITN - 1803	75 21.660 S, 164 44.581 E	71	AQD	9929	12/3/2018	4/1/2019	600		
		73	SBE37SM	16537	12/3/2018	4/1/2019	300		
		114	SBE56	4855	12/3/2018	4/1/2019	20		
		154	SBE56	4856	12/3/2018	4/1/2019	20		
		194	SBE56	6464	12/3/2018	4/1/2019	20		
		224	SBE56	8011	12/3/2018	4/1/2019	20		
		263	AQD	14283	12/3/2018	4/1/2019	600		
		274	SBE37SM	16566	12/3/2018	4/1/2019	300		
		666	AQD	14372	12/3/2018	4/1/2019	600		
		670	SBE37SM	16568	12/3/2018	4/1/2019	300		
DITN - 1901	75 20.914 S, 164 48.951 E	67	AQD	9929	4/1/2019	10/9/2019	600		
		71	SBE37SM	3431	7/1/2019	13/3/2020	300		
		112	SBE56	2098	7/1/2019	17/3/2020	30		
		152	SBE56	2115	7/1/2019	17/3/2020	30		
		192	SBE56	4851	7/1/2019	17/3/2020	30		
		232	SBE56	4857	7/1/2019	17/3/2020	30		
		255	AQD	14283	4/1/2019	17/3/2020	600		
		271	SBE37SM	2443	7/1/2019	10/3/2020	120		
		649	AQD	14372	4/1/2019	8/9/2019	600		
		647	SBE37SM	2444	-	-	-		Faulty data - removed
DITN - 2003	75 20.958 S, 164 49.021 E	53	SBE37SM	2444	-	-	-	Instrument flooded - no data	
		54	AQD	14292	18/3/2020	22/7/2020	600		
		95	SBE56	4855	18/3/2020	15/3/2022	60		
		135	SBE56	4856	18/3/2020	15/3/2022	60		
		175	SBE56	6464	18/3/2020	15/3/2022	60		
		215	SBE56	8011	18/3/2020	12/2/2022	60		
		269	SBE37SM	16413	18/3/2020	15/3/2022	300		No S data
		252	AQD	14289	18/3/2020	14/8/2020	600		
		667	SBE37SM	16417	18/3/2020	15/3/2022	300		
		671	AQD	14288	18/3/2020	24/8/2020	600		

Table 3.

$$\Delta S_{t_1} = S_{CTD_{dep}} - S_{mooring_{t_1}} \quad (1)$$

$$\Delta S_{t_f} = S_{CTD_{rec}} - S_{mooring_{t_f}} \quad (2)$$

$$S(t)_{calibrated} = S(t)_{mooring} + \Delta S_{t_1} + \frac{\Delta S_{t_f} - \Delta S_{t_1}}{N} \cdot t, \quad (3)$$

Instrument	Location	Depth [m]	Type	sn	start	end	interval [s]	data quality
DITD - 1702	75 16.542 S,	1225	SBE37SM	15273	8/2/2017	6/3/2018	120	
	164 04.038 E	1239	AQD	13041	8/2/2017	6/3/2018	900	
DITD - 1803	75 16.640 S, 164 04.260 E	1122	SBE37SM	15273	10/3/2018	3/1/2019	60	
		1145	AQD	9930	10/3/2018	3/1/2019	600	
		1218	SBE37SM	15242	10/3/2018	3/1/2019	180	
		1244	AQD	6162	10/3/2018	22/6/2018	600	
DITD - 1901	75 16.597 S, 164 04.198 E	1219	SBE37SM	4840	6/1/2019	17/3/2020	120	
		1221	AQD	9930	3/1/2019	12/3/2020	600	
DITD - 2003	75 16.681 S, 164 03.616 E	1213	AQD	14383	18/3/2020	1/8/2020	600	
		1218	SBE37SM	15273	18/3/2020	17/3/2022	300	
DITD - 2211	75 16.667 S, 164 3.642 E	1204	AQD	14383	10/12/2022	21/1/2024	600	
		1205	SBE37SM	20388	10/12/2022	21/1/2024	300	
DITD - 2401	75 16.660 S, 164 3.610 E	1206	SBE37SM	16419	21/1/2024	8/12/2024	300	
		1214	AQD	9929	21/1/2024	8/12/2024	600	

Table 4.

160 where $S_{CTD_{dep}}$ is the salinity measured by the CTD at depth of the instrument close to the time of deployment, $S_{CTD_{rec}}$
is the salinity measured by the CTD at depth of the instrument close to the time of recovery of the mooring, $S_{mooring_{t_1}}$
is the salinity measured by the mooring just after it is deployed, $S_{mooring_{t_f}}$ is the salinity measured by the mooring just
before it is recovered and N is the number of observations made by the mooring. The mooring timeseries is only calibrated if
 ΔS_{t_1} or ΔS_{t_f} is larger than $0.003psu$. This value is chosen as it is the lower bound of the uncertainties within SBE37SM(P)
165 CTD instruments. In case that the instrument stopped recording before recovery, the calibration is done by $S(t)_{calibrated} =$
 $S(t)_{mooring} + \Delta S_{t_1}$. The temperature sensors were not adjusted post-deployment. Sea-Bird temperature sensors are highly
stable and exhibit substantially lower drift than salinity, which is derived from conductivity and temperature. Applying a post-
deployment temperature calibration to the SBE37SM(P) and SBE56 instruments would therefore likely introduce additional
noise rather than improve data quality (Sea-Bird Scientific, n.d.).

170 3 Oceanographic data

This section lists all the available data measured by the instruments on the DITx moorings in Terra Nova Bay. The mooring is
referred to as [mooring][deployment year][deployment month], for example DITN1412. Details about the measurements are
described per variable in the corresponding subsections, including the depth and period where observations are absent or need
to be treated with caution due to faulty instruments or depleted batteries. The observational daily multi-year means are shown
175 for the salinity, temperature, density and speed for the DITN and DITD mooring. The multi-year means are not shown for the
observations of DITS as this mooring was only maintained for 3 years, with instruments at varying depths.

3.1 CTD results

Pressure is recorded by the Aquadopp and the MicroCAT, SBEs; the measurements per depth are plotted in Figure 5 (DITN: a-c , DITS: d - f, DITD: g) . The depth at which the variables are measured, as described in Table 3, 4 and 5, are the mean values of the pressure-derived depth values. This mean is calculated by the median of the pressure derived depth values, to account for the mooring deflection due to strong wind-induced currents. The mean depth for instruments that do not record the pressure is calculated based on linear interpolation and spacing between two known depths - i.e. between the bed anchor, and an SBE37SM(P). The instrument depths vary between deployments, so combining the datasets requires caution to account for differences in measurement levels.

185

The pressure derived depth also varies between deployments, as the depth varies, in the order of a few meters, due to the exact location of the mooring anchor, therefore the depth of the mooring anchor changes slightly each time the mooring is retrieved and deployed again. The pressure data shows bigger spikes in the instruments closer to the surface compared to the instruments

Instrument	Location	Depth [m]	Type	sn	start	end	interval [s]	data quality
DITS - 1702	75 29.305 S, 163 10.461 E	191	RCM9	647	12/2/2017	8/3/2018	3600	faulty P & S data removed
		192	SBE37SM	7227	12/2/2017	8/3/2018	300	
		233	SBE56	4855	12/2/2017	24/10/2017	10	
		273	SBE56	4856	12/2/2017	2/10/2017	10	
		313	SBE56	4857	12/2/2017	21/10/2017	10	
		353	SBE56	6464	12/2/2017	10/11/2017	10	
		383	SBE37SM	1627	12/2/2017	8/3/2018	300	
		384	RCM9	845	12/2/2017	8/3/2018	3600	
		1087	RCM9	847	12/2/2017	8/3/2018	3600	
		1088	SBE37SM	7284	12/2/2017	8/3/2018	600	
DITS - 1803	75 29.313 S, 163 12.251 E	47	AQD	14288	4/3/2018	2020-02-19	600s	
		63	SBE37SM	15239	10/3/2018	14/6/2018	20s	
		88	SBE56	4673	9/3/2018	28/1/2020	20	
		128	SBE56	2089	9/3/2018	28/1/2020	20	
		168	SBE56	4852	9/3/2018	28/1/2020	20	
		208	SBE56	4854	9/3/2018	28/1/2020	20	
		220	AQD	14289	4/3/2018	28/1/2020	600	
		339	SBE37SM	15240	10/3/2018	18/6/2018	20	
		1027	AQD	14290	4/3/2018	28/1/2020	600	
				1458	SBE37SM	15257	10/3/2018	

Table 5.

190 closer to the bottom. These spikes are not removed from the data as they are caused by a increase in depth when the mooring line gets pulled down due to drag imposed by currents. This has no significant impact on the mean and median of the pressure derived depth, as they are short lived (order of hours) events.

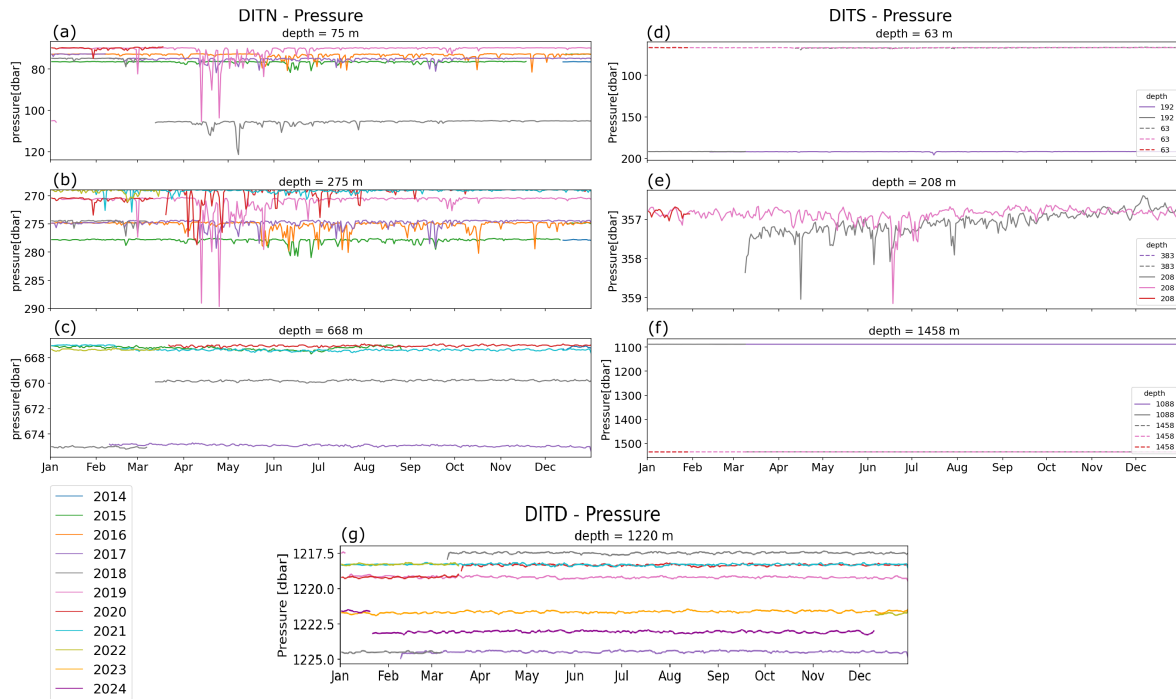


Figure 5. The pressure measured by the (a) - (c) DITN at ~ 75 m, ~ 275 m and ~ 668 m depth, (d) - (f) by the DITS at ~ 48 m, ~ 192 m, ~ 220 m, ~ 1027 m and ~ 1088 m depth and (g) by the DITD ~ 1220 m depth.

All SBE37SM(P), SBE56 and Aquadopp instruments measure the temperature. The depths of these instruments per mooring can be found in Tables 3, 4 and 5. Figure 6 shows the temperatures for each of the instruments (DITN: 6a-c, DITS: 6d-f, DITD:6g). The accuracy of the Sea-Bird instrument are significantly better (0.002°C) than the Aquadopp (0.01°C) and the RCM9 (0.05°C) as shown in Table 1. Neither the SBEs, Aquadopp or RCM9 temperature sensors are calibrated as described in Section 2.1.

The temperatures measured in the top 400 m, show a clear seasonal signal, decreasing with depth, as shown in Figure 6a,b,d&e. The temperature measured by the DITN near the surface at ~ 75 m depth (Figure 6a increases from November, peaking at the end of February, it decreases during the Autumn months from March until June and during the winter months, the temperatures are $\sim -1.9^{\circ}\text{C}$ and show the smallest variability at this mooring. In the Geiki inlet where the DITS is located, the temperature in the top 100 m (Figure 6d) increases from the end of December, peak in February, and decreases until April where temperatures

show low variability throughout the winter and spring. At 275 m depth at the DITN (Figure 6b) and at 208 m at the DITS
205 site (Figure 6e), the temperature does not increase until late February. During April the highest temperatures of ~ -1.2 to
 -1.7°C are recorded and they start to drop again during May and June. The winter period starts in July at the DITN site and
in May at the DITS site with temperatures $\sim -1.9^{\circ}\text{C}$ with super-cooled water reaching $< -2.0^{\circ}\text{C}$. Near the bottom (Figure
6c,g) temperatures range between -1.87°C and -1.91°C , there is a decrease between July and November at the DITD and
DITN locations and no clear seasonal signal at the DITS site (Figure 6f). There is a strong temperature increase between end
210 of April and start of May measured by the SBE37SM DITS1803_15239 at 63 m depth (Figure 6d) and the SBE56 thermistor
DITS1803_4854 at 208 m depth (Figure 6e). Because this signal is measured two different instruments at two different depths,
it is not removed from the final dataset, but should be treated with caution. Sudden large temperature changes (spikes) that
last longer than 1 hr are not removed from the dataset as the polynya is a highly active environment and sudden temperature
changes can occur.

215

The temperatures are measured correctly for most of the instruments and moorings. The measurements that need to be treated
with caution, are absent, or ignored due to faulty instruments are presented in Table 3, 4 & 5. Aquadopp c1901DITN_9929
at 71 m depth (Figure 6a) shows a sudden jump in temperature on 22/8/2019. At the same time as the sudden temperature
increase, the pressure increases to 90 dbar at 15:30 and decreases again to 68 dbar at 16:15 (Figure 5a), while the temperature
220 does not go back to the values before the sudden increase. This could indicate that the instrument got hit by an iceberg and
possibly broke the temperature sensor. The temperature data after 22/8/2019T15:30 is removed in the final dataset.

The salinity is measured in PSU indirectly by the SMBE37SM using conductivity and temperature, and converted to absolute
salinity [g/kg] in this paper. At DITN near the surface at ~ 75 m depth (Figure 7a), the salinity decreases in the summer from
225 the middle of January from 34.9psu to 34.2psu. At ~ 275 m depth (Figure 7b), the salinity oscillates with the highest salinity
in September and the lowest salinity in May. Close to the bottom, there is no obvious seasonal signal. In the Drygalski Basin,
measured by the DITD (Figure 7g), the salinity decreases slowly from the end of Autumn, with a sharp increase between
September and October. The SBE37SM instruments on the DITS1803 mooring, measuring the salinity either did not record
any data or stopped early. The salinity measurements are plotted in Figure 7.

230

The in-situ density is measured for DITN at 75, 275 & 668 m depth, on DITD at 1220 m, on DITD1803 at 1120 m, on
DITS1702 at 190, 390 and 1090 m, and on DITS1803 at 48, 240 and 1050 m. The MicroCAT did not record any density
data from the DITN1902. Also there is no density data recorded on the 15/12 mooring at 275 m (SBE37SM724) and 668 m
(SBE37SM5838) depth. The missing density data can be calculated using the TEOS10 function with the salinity, temperature
235 and pressure. The measured in-situ density on the DITN1902 mooring at 668 m depth, is faulty, as it is calculated with the
salinity and temperature, which was not recorded correctly. The same applies to the DITS1803 mooring data at 48 and 240 m
depth.

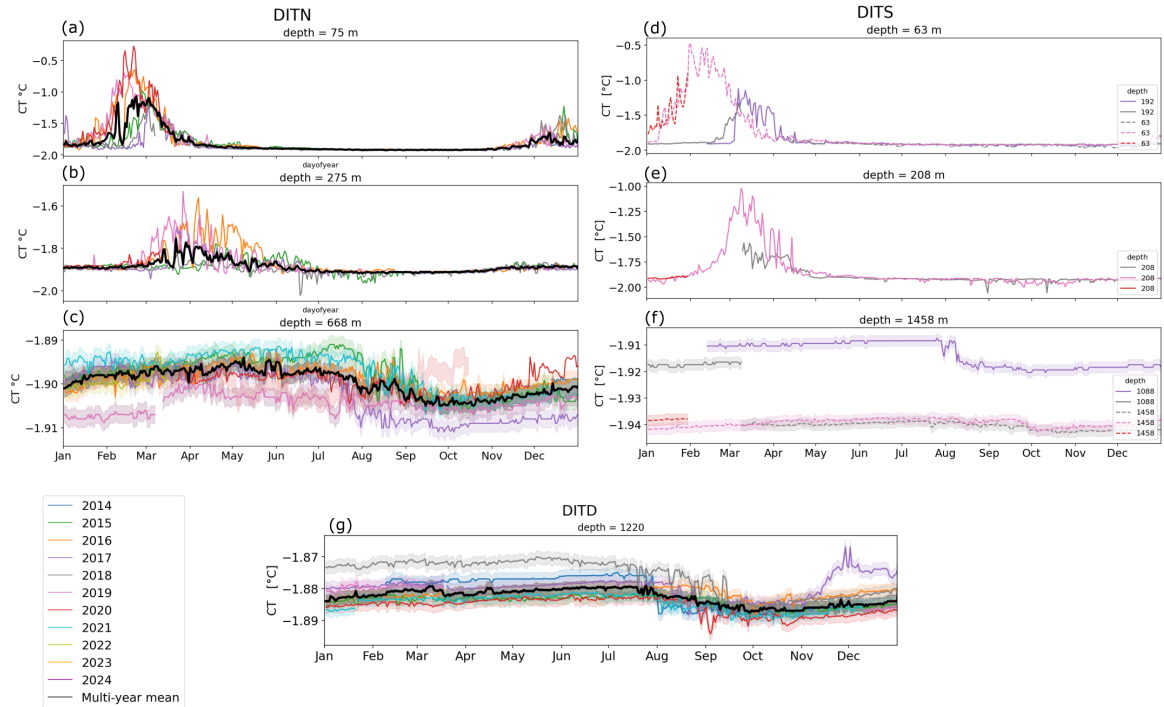


Figure 6. The temperature measured (a) - (c) by the DITN at ~ 75 m, ~ 275 m and ~ 668 m depth, (d) - (f) by the DITS at ~ 48 m, ~ 63 m, ~ 88 m ~ 192 m, ~ 208 m, ~ 228 m, ~ 383 m, ~ 1064 m, ~ 1088 m and ~ 1458 m depth and (g) by the DITD ~ 1220 m depth. The observational multi-year mean is represented by the black line for DITN and DITD. DITS does not have enough observations to compute a multi-year mean. The calibration error and sensor drift are represented in the as uncertainty bands, based on the uncertainty of the corresponding instrument.

3.1.1 Water masses

240 We observe the following water masses in Terra Nova Bay near the Drygalski Ice Tongue: High Salinity Shelf Water (HSSW),
 defined as $\rho > 1028.00 \text{ kgm}^{-3}$, Terra Nova Bay ice shelf water (TISW) where the temperature is below the surface freez-
 ing temperature $CT < \sim -1.94^\circ\text{C}$ depending on salinity, and Antarctic Surface Water (ASW) $> -1.7^\circ\text{C}$ (Yoon et al., 2020;
 Friedrichs et al., 2022). The TS-diagrams for the three depths that measure salinity in DITN and at DITD are shown in Figure
 8a - l and 8m-p respectively. The variability of the top half of the water column, up to 275 m depth (Figure 8a-h), is forced
 245 by surface processes. The temperature and salinity response in the mid water-column (Figure 8e-h) is shifted forward in time
 compared to the subsurface; in spring, we first observe a freshening and increase in temperature at 75 m depth (Figure 8d),
 while fresher and warmer water masses don't reach deeper within the water column at 275 m depth (Figure 8e) until sum-
 mer. In Autumn, the subsurface (Figure 8b) also cools and increases in salinity before the mid water column (Figure 8f,g).
 The mixed layer depth rapidly increases between March and May and is assumed to be homogeneously mixed throughout the

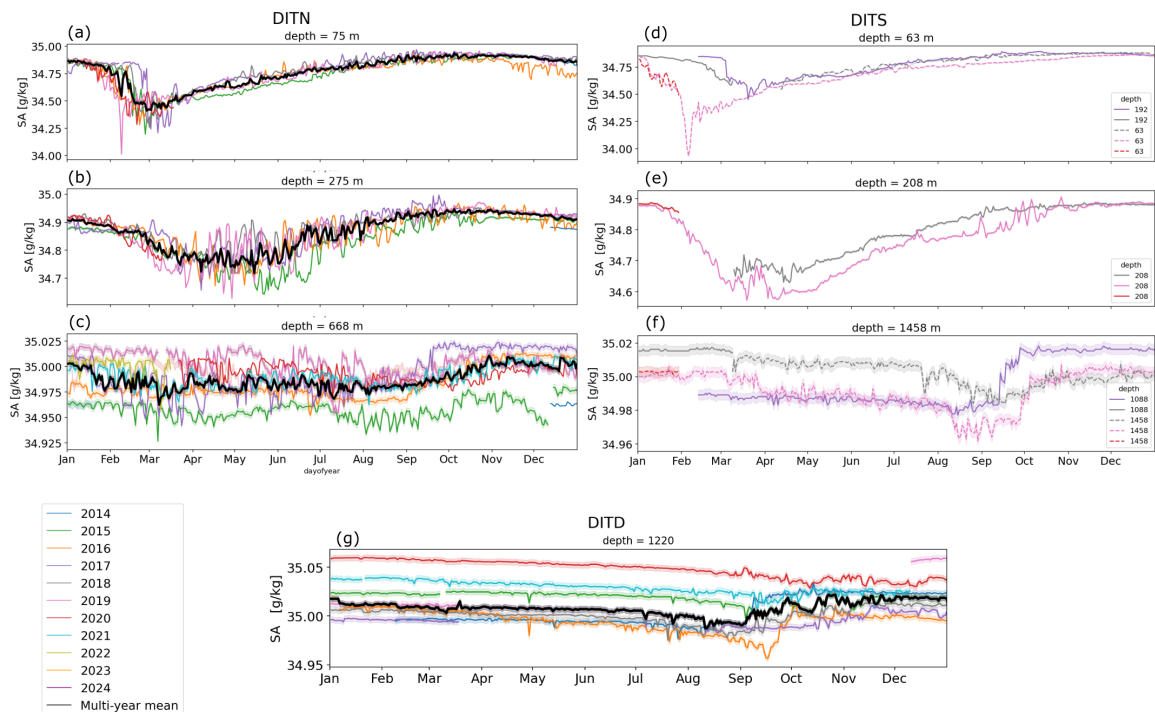


Figure 7. The salinity and 0.01 g/kg uncertainty measured (a) - (c) by the DITN at ~ 75 m, ~ 275 m and ~ 668 m depth, (d) - (f) by the DITS at ~ 63 m, ~ 192 m, ~ 208 m, ~ 1088 m and ~ 1458 m depth and (g) by the DITD ~ 1220 m depth . The observational multi-year mean is represented by the black line for DITN and DITD. DITS does not have enough observations to compute a multi-year mean. The calibration errors and sensor drift are represented in the as uncertainty bands, based on the uncertainty of the corresponding instrument.

250 winter mass (Yoon et al., 2020), when HSSW is formed through sea ice formation during katabatic wind events. However, the HSSW formed in the eastern Terra Nova Bay does not convect all the way to the bottom, as the salinity observed in the top half of the water column (Figure 7a,b & Figure 8a,h) is fresher than observed at the bottom instrument of DITN (Figure 7c & Figure 8i - l) and the annual salinity increase is observed much later, between September and October, compared to the top half of the water column, as shown in Figure 7a,b,d & e. Yoon et al. (2020) found a cyclonic circulation between 400 - 700 m
 255 depth in CTD and mooring observations (DITN, DITD and Mooring D) that advects HSSW, formed in front of the Nansen Ice Shelf, to the bottom instrument of DITN and the Drygalski Basin.

TISW is observed by DITN in the top half of the water column, where the Drygalski Ice Tongue extends to ~ 200 - 400 m depth. In the subsurface at 75 m depth (Figure 6a & Figure 8a - d), TISW is observed during winter and spring (Figure 8c,d), while at
 260 275 m depth (Figure 8e,f) it is observed between summer and autumn, but with large interannual variability. This is in contrast to the Terra Nova Bay wide CTD observations in Yoon et al. (2020) that observed TISW at 275 m depth, however, they did find that the presence of TISW was dependent on the observation period. DITN is located close to the DIT, and the TISW observed

by this mooring likely originates from water masses mixed with basal melt water from the ice tongue. Further study is needed to confirm this, as Yoon et al. (2020) found that TISW formed under the Nansen Ice Shelf is advected in a cyclonic circulation similar to the HSSW.

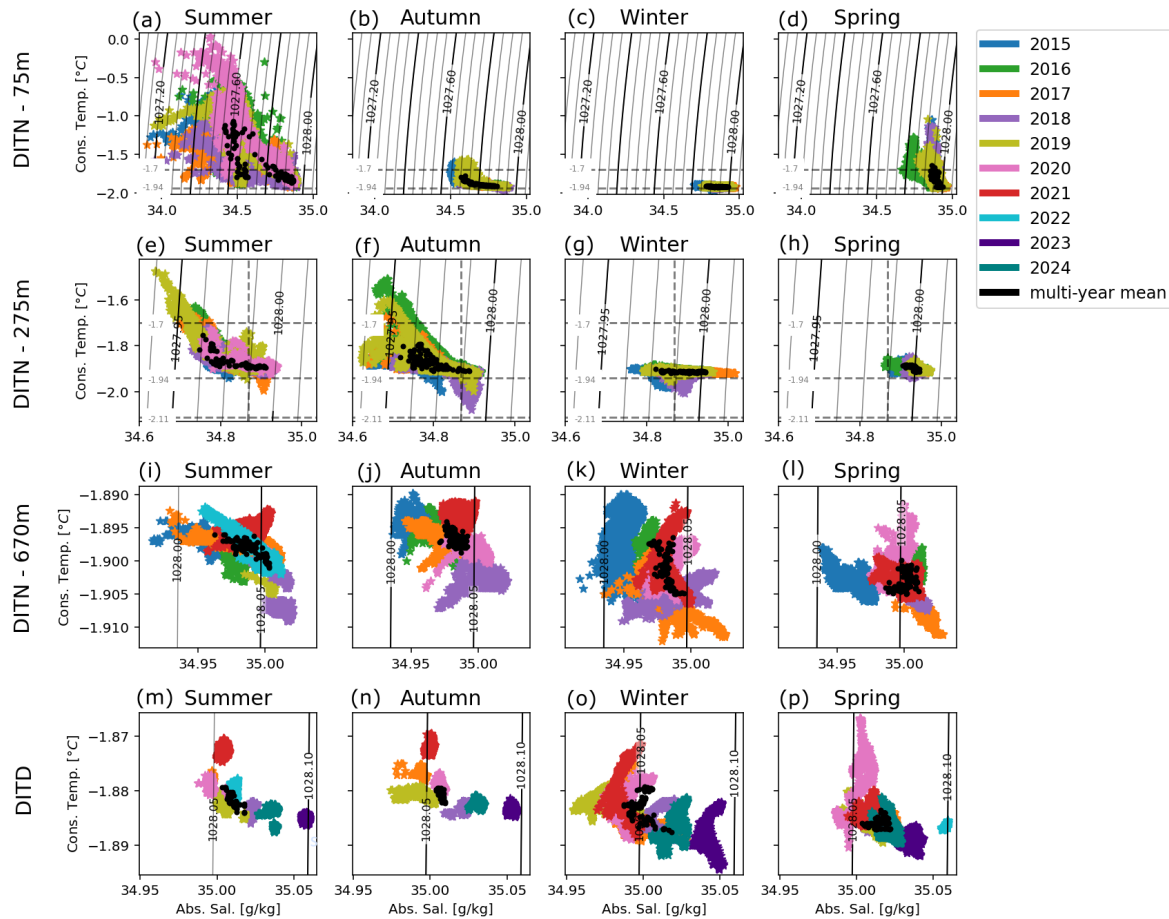


Figure 8. The absolute salinity versus the conserved temperature per season for each depth, colored by year. The daily multi-year mean over the observed years is plotted in black. Summer is defined as the period from Jan-1 until Apr-1, Autumn from Apr-1 until Jul-1, Winter from Jul-1 until Oct-1 and Spring from Oct-1 until Jan-1. The isopycnals are plotted at 0.05 kgm^{-3} intervals, with inline values. The isotherms define the ISW ($CT < T_{fs}$) and AAWS ($CT > -1.7[^\circ\text{C}]$).

3.2 Current meter results

The speed and direction of the current is measured with the RCM9 and Aquadopp instruments. On the DITN at 74, 76, 265, 274, 670 & 672 m depth. The RCM9 was installed on the DITN1412 & DITN1512 mooring at 74, 274 & 272 m depth and 270 DITN1702 mooring at 74, 274 & 342 m depth and the Aquadopp at 76, 265 & 670 m depth from the DITN1702 mooring onwards. The DITD measures the currents with the Aquadopp at 1240 m depth. The currents are measured on the DITS1702 at 190, 390 and 1090 m depth with the RCM9, and on the DITS1803 50, 230 and 1060 m depth with the Aquadopp.

Figure 9 shows the hourly means of the current speed for each of the moorings. The current direction is corrected for the magnetic declination at the position of the mooring.

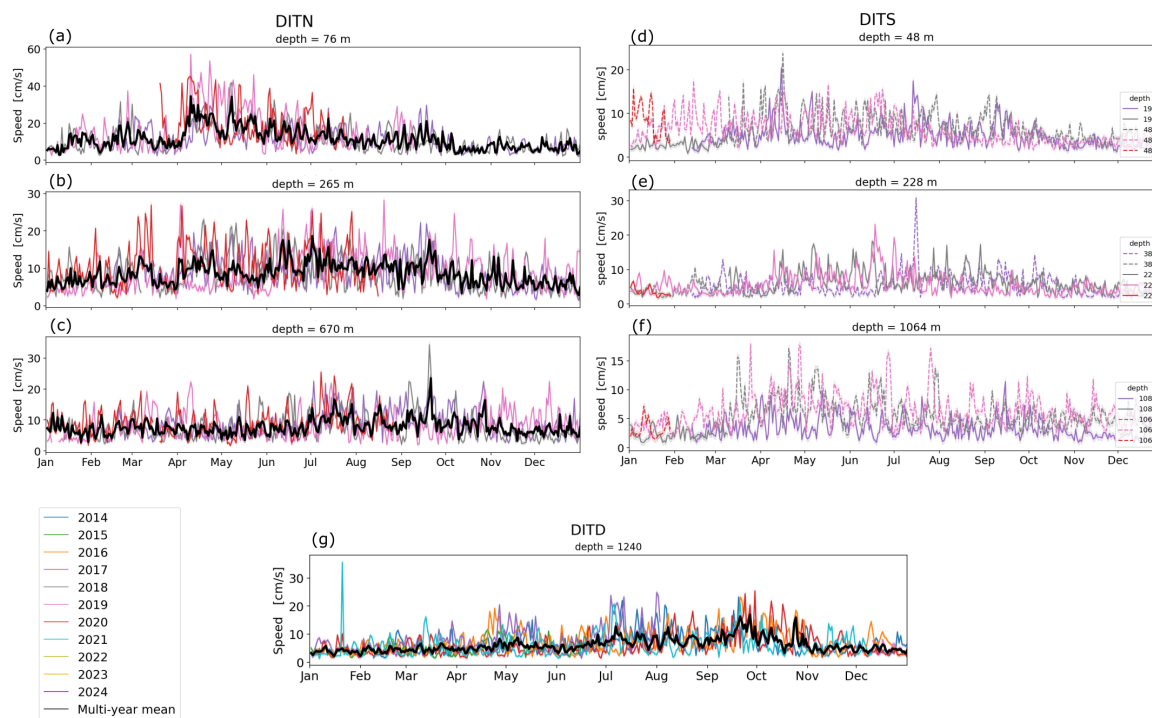


Figure 9. The current speed measured (a) by the DITN at ~ 76 m, ~ 265 m, and ~ 670 m depth, (b) by the DITS at ~ 48 m, ~ 191 m, ~ 228 m, ~ 384 m, ~ 1064 m and ~ 1087 m depth and (c) by the DITD ~ 1240 m depth. The observational multi-year mean is represented by the black line for DITN and DITD. DITS does not have enough observations to compute a multi-year mean. The calibration errors and sensor drift are represented in the as uncertainty bands, based on the uncertainty of the corresponding instrument.

The prevailing direction of the flow shows in Figure 10 measured by DITN is westerly near the surface at ~ 75 m depth (Figure 10a) and in the middle of the water column at ~ 275 m depth (Figure 10b). At the bottom at a depth of 670 meters (Figure

10c), the current direction is very variable with a slight south westerly tendency. The flow at DITD (Figure 10d) has a westward
 280 tendency, ranging between north west and south west or in north east direction. The bottom instrument of DITN and DITD
 show the largest variability, while the subsurface shows the smallest variability. This preferred westerly flow near the surface
 corresponds with the deflection of the Victoria Land Coastal current deflection observed in satellite data [(Moctezuma-Flores
 et al., 2017)].

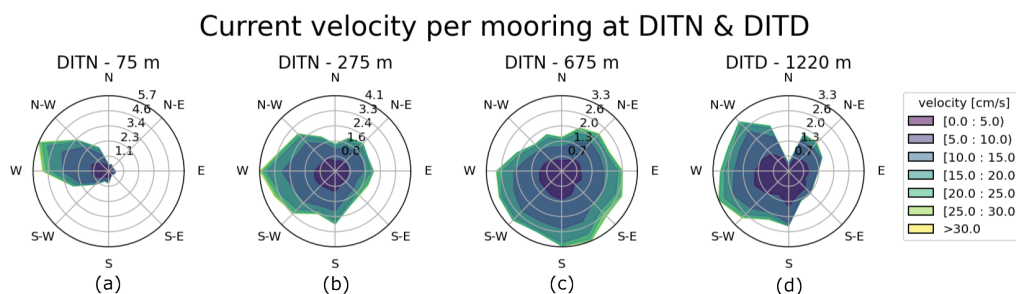


Figure 10. The currents measured by the three DITN aquadopps and the DITD are plotted per instrument. The contours represent the direction and speed of the currents of the total observed period. The radius of the bar represents the frequency of the occurrence.

285 The heading, roll and pitch are measured with the Aquadopp on the DITN1702 onwards at 76, 265 & 670 m depth, at 1145
 & 1240 m on the DITD moorings and at 50, 230 and 1070 m on DITS1803. The heading is the rotation along the z-axis, the
 pitch along the x-axis and the roll along the y-axis. The heading, roll and pitch data can be used to study the movement of
 the mooring. The set-up, lengths between the instrument connections and length of the chains of the mooring can explain the
 variability in between mooring deployments.

290 3.3 Spectral analysis

A spectral analysis is performed to assess the dominant timescales of the observed velocities and pressure. The power spectral
 density (Figure 11) shows two clear peaks at 1 and 2 cycles per day in the pressure data (Figure 11e,f) in the bottom two
 instruments, corresponding to the diurnal and semi-diurnal tidal constituents, with the diurnal tide the dominant tidal frequency
 in the region. Near the surface (Figure 11d) this signal is not as profound, suggesting the pressure is affected by other processes
 295 like surface gravity waves induced by wind that operate around the frequency of the tides. The spectral analysis of the speed
 data only shows a peak at one cycle per day (Figure 11a) that corresponds with the tidal motion; at greater depth (Figure
 11b,c) these peaks are absent. The tidal constituents are not clearly visible in the speed data, likely because eddies are shed
 from the ice tongue and advected past the instruments, while the background currents driven by tidal motion move around
 the ice tongue. At greater depth, the diurnal and semi-diurnal tidal constituents are clearly evident in the pressure spectral
 300 analysis, reflecting the dominance of barotropic tidal forcing where surface effects and transient processes such as wind or ice
 interactions are minimal. A distinct secondary peak is observed near 0.2 cycles per day (Figure 11a), indicating variability on

a 3-5 day timescales. These lower scale fluctuations represent the inertial and sub-inertial variability like eddies and synoptic forcing like storms and katabatic wind events.

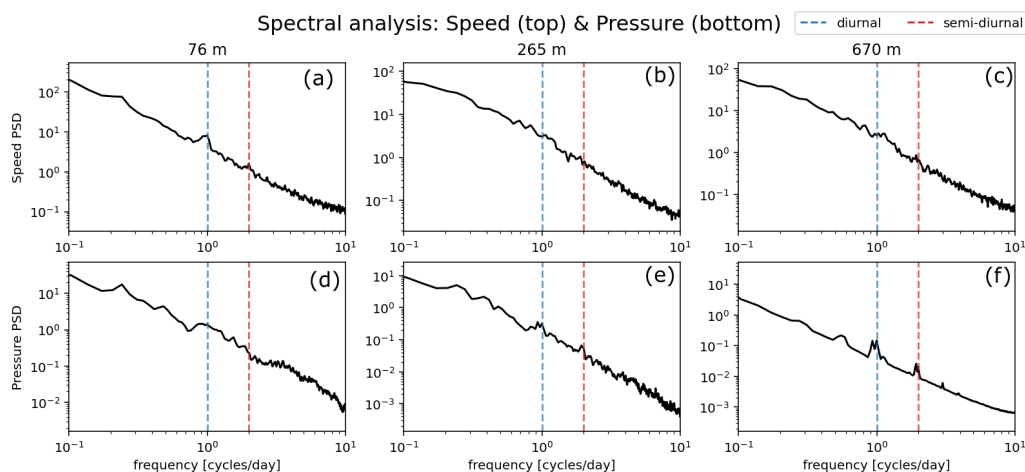


Figure 11. The spectral density analysis of the speed (top row) and pressure (bottom row) data of all years at the current meters at ~ 76 m, ~ 265 m and ~ 670 m depth. Vertical dashed lines indicate diurnal (blue) and semi-diurnal (red) tidal frequencies.

4 Discussion and Conclusions

305 This paper shows the data collected by three mooring around the Drygalski Ice Tongue in Terra Nova Bay between December 2014 and December 2024. The Drygalski Ice Tongue is a prominent feature in Terra Nova Bay and blocks the inflow of sea ice from the south, enabling it to operate as a polynya during the colder months of the year. The water masses formed in Terra Nova Bay interact with the Drygalski Ice Tongue and variability in these water masses is relevant for understanding ocean conditions in its vicinity and broader ice-ocean interactions (Wang et al., 2023). Long-term observations provide important

310 context for monitoring hydrographic variability close to the Drygalski Ice Tongue. As the Drygalski Ice Tongue also extends into the water column, it also affects the circulation and advection of water masses within Terra Nova Bay and the exchange below the ice tongue (Stevens et al., 2024). A modelling study that represented a polynya similar to Terra Nova Bay done by Xu et al. (2023), found that an ice tongue in a coastal polynya changes the circulation patterns compared to polynya that is not bound by an ice tongue. They observed a surface flow along the ice tongue towards the ice shelf front, which corresponds

315 with the westerly flow observed at the subsurface instrument of DITN. Together, these observations provide in-situ context for interpreting seasonal and interannual variability of the circulation patterns close to the ice tongue.

4.1 Outlook and uses of data

The described hydrographic mooring time series, presented in this paper, is a valuable tool to increase our understanding of the highly dynamic polynya system. Comparing this data set with other observations in Terra Nova Bay, helps with the horizontal extent of the polynya dynamics and variability. The length of the observations closer to the surface, provides insight into the drivers of and interannual variability of water mass formation processes. This long-term dataset constrains variability associated with atmospheric conditions, sea ice dynamics, and ocean circulation patterns, that influence the timing, amount, and properties of HSSW rather than allowing direct attribution and supports future investigation of how the Drygalski Ice Tongue itself may influence these processes. We aim to determine the origin of water masses observed near the Drygalski Ice Tongue during the winter months when HSSW is formed while bay-wide CTD observations are impossible. In future work we also aim to use idealised and regional models to complement the observational dataset.

The datasets from DITN and DITS are also valuable for biological applications. Both DITN and DITS include instruments located within the euphotic zone, allowing for the analysis of the mixed layer depth and its variability. Due to close proximity of DITN and DITS to the Drygalski Ice Tongue, these datasets offer an opportunity to investigate oceanographic conditions in the vicinity of the ice tongue that are relevant for understanding ice-ocean interaction, rather than assessing ice-tongue stability or evolution. These moorings can give an in-situ oceanographic perspective that complements changes observed with radar and satellite data. When combined with radar and satellite imagery, the in-situ data provide a complementary oceanographic perspective, enhancing our understanding of ice-ocean interactions and supporting interdisciplinary studies linking ocean physics, glaciology, and marine biology.

Code and data availability. This paper provides a detailed description of the temporal coverage of the dataset, which consists of a near-continuous high-temporal-resolution time series of currents, temperature, and salinity from December 2014 to December 2024. The methodology adopted for settings, data recording, and quality control ensures the dataset's compliance and consistency. Although the dataset currently ends in December 2024, monitoring activities are ongoing. Future data from this hydrographic timeseries will be added to an updated version of the repository as future moorings are recovered. All coding used to make the datafiles are uploaded to Github: https://github.com/Livcornelissen/DIT_mooringdata/tree/main. The data of the three hydrographic moorings are uploaded as netcdf files to SEANOE in DOI:10.17882/102640 (Cornelissen et al., 2025)

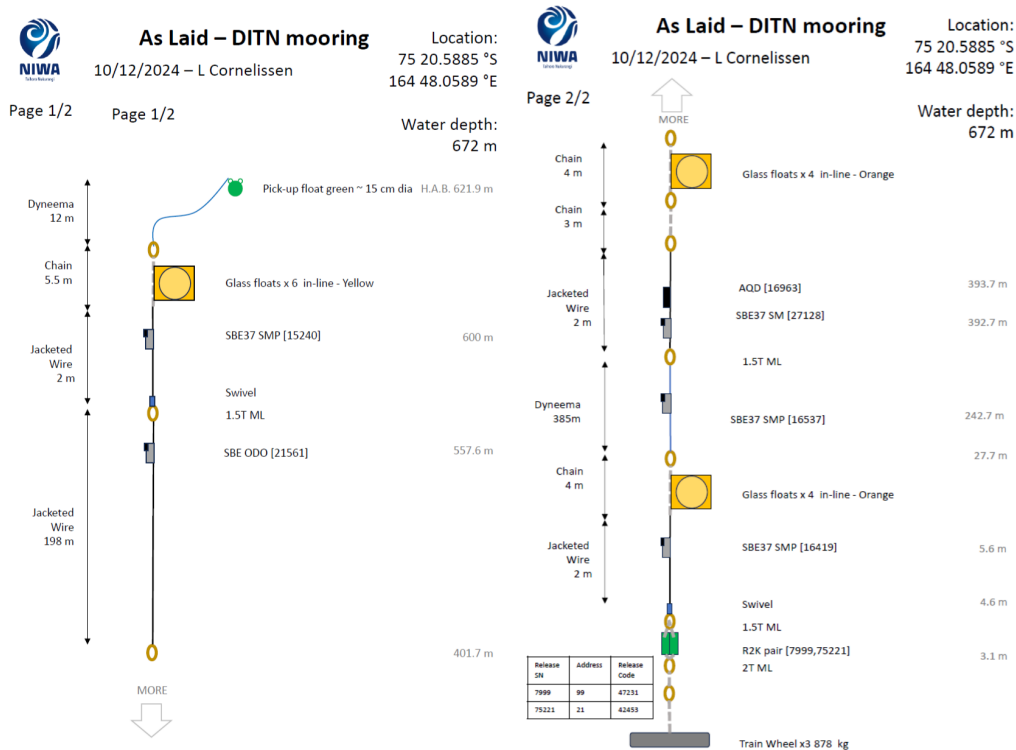


Figure A1.

Appendix A: Additional figures

345 *Author contributions.* The dataset was assembled and checked by LC. The deployment and recovery of the moorings were led by JMc, BG, FE, CJZ, SY, STY and LC on various voyages with the assistance of the *Araon* deck crew. The timeseries was initiated by CS, WSL and CJZ. LC wrote up the manuscript and all other co-authors helped improve it.

Competing interests. The authors declare that they have no conflict of interest.

350 *Acknowledgements.* The authors wish to thank the Korea Polar Research Institute (KOPRI), the New Zealand Antarctic Research Institute, the N.Z. Antarctic Science Platform and Antarctica New Zealand for support. We especially thank the crew of the IBRV *Araon*. The mooring instruments are provided by the NIWA Capex Program. This paper forms a contribution to the N.Z. Antarctic Science Platform (ANTA1801). We thank Gary Wilson and Richard Levy for their support in initiating this work. In addition, we acknowledge Pierpaolo Falco and Pasquale

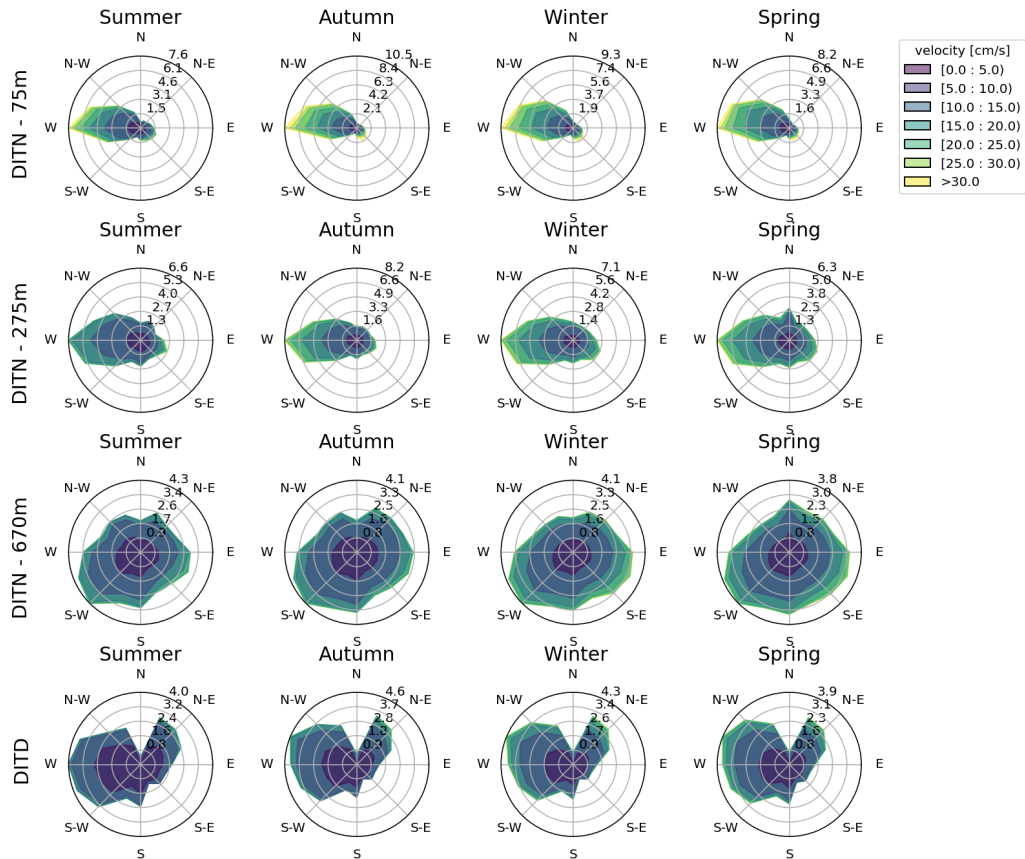


Figure A2. The currents measured by the three DITN aquadopps and the DITD are plotted per instrument, per season. The contours represent the direction and speed of the currents of the total observed period. The radius of the bar represents the frequency of the occurrence.

Castagno who assisted in recovery of the DITS mooring with the *Laura Bassi*. SY and WSL are supported by the Korea Institute of Marine Science & Technology Promotion (KIMST) funded by the Ministry of Oceans and Fisheries (RS-2023-00256677; PM25020).

355 **References**

- Barber, D., & Massom, R. (2007). Chapter 1 - The Role of Sea Ice in Arctic and Antarctic Polynyas. *In Elsevier oceanography series (pp. 1–54)*. [https://doi.org/10.1016/s0422-9894\(06\)74001-6](https://doi.org/10.1016/s0422-9894(06)74001-6)
- Bianchi, N. C., Chiappini, N. M., Tabacco, N. I. E., Passerini, N. A., Zirizzotti, N. A., & Zuccheretti, N. E. (2001). Morphology of bottom surfaces of glacier ice tongues in the East Antarctic region. *Annals of Geophysics, 44(1)*. <https://doi.org/10.4401/ag-3609>
- 360 Broecker, W. S., Peteet, D. M., & Rind, D. 1985. Does the ocean–atmosphere system have more than one stable mode of operation? *Nature, 315(6014), 21–26* <https://doi.org/10.1038/315021a0>
- Budillon, G., & Spezie, G. 2000. Thermohaline structure and variability in the Terra Nova Bay polynya, Ross Sea. *Antarctic Science, 12(4), 493–508*. <https://doi.org/10.1017/s0954102000000572>
- Castagno, P., Capozzi, V., DiTullio, G. R., Falco, P., Fusco, G., Rintoul, S. R., Spezie, G., & Budillon, G. (2019). Rebound of shelf water salinity in the Ross Sea. *Nature Communications, 10(1)*. <https://doi.org/10.1038/s41467-019-13083-8>
- 365 Cornelissen, L., Yun, S., McInerney, J., Grant, B., Elliot, F., Yoon, S., Zappa C.J., Lee, W.S. & Stevens, C. (2025). A decade-long hydrographic mooring dataset near the Drygalski Ice Tongue, Terra Nova Bay, Antarctica. *SEANOE*. <https://doi.org/10.17882/102640>
- Frezzotti, M., & Mabin, M. 1994. 20th century behaviour of Drygalski Ice Tongue, Ross Sea, Antarctica. *Annals of Glaciology, 20(1), 397–400*. <https://doi.org/10.3189/172756494794587492>
- 370 Friedrichs, D. M., McInerney, J. B. T., Oldroyd, H. J., Lee, W. S., Yun, S., Yoon, S., Stevens, C. L., Zappa, C. J., Dow, C. F., Mueller, D., Steiner, O. S., & Forrest, A. L. (2022b). Observations of submesoscale eddy-driven heat transport at an ice shelf calving front. *Communications Earth & Environment, 3(1)*. <https://doi.org/10.1038/s43247-022-00460-3>
- Gomez-Fell, R., Marsh, O. J., Rack, W., Wild, C. T., & Purdie, H. (2023). Basal mass balance and prevalence of ice tongues in the Western Ross Sea. *Frontiers in Earth Science, 11*. <https://doi.org/10.3389/feart.2023.1057761>
- 375 Gordon, A. L., Orsi, A. H., Muench, R., Huber, B. A., Zambianchi, E., & Visbeck, M. 2009. Western Ross Sea continental slope gravity currents. *Deep Sea Research Part II Topical Studies in Oceanography, 56(13–14), 796–817*. <https://doi.org/10.1016/j.dsr2.2008.10.037>
- Gossart, A., Malyarenko, A., Cornelissen, L., Stevens, C., Miller, U., Zappa, C. J., Luca, N., Castagno, P., and Budillon, G.: Representation of polynyas in the Ross Sea coupled atmosphere–sea ice–ocean model P-SKRIPsv2, EGUsphere [preprint], <https://doi.org/10.5194/egusphere-2025-4332>, 2025.
- 380 Indrigo C, Dow CF, Greenbaum JS, Morlighem M (2021). Drygalski Ice Tongue stability influenced by rift formation and ice morphology. *Journal of Glaciology 67(262), 243–252*. <https://doi.org/10.1017/jog.2020.9>
- Killworth, P. D. 1983. Deep convection in the World Ocean. *Reviews of Geophysics, 21(1), 1–26*. <https://doi.org/10.1029/rg021i001p00001>
- Malyarenko, A., Gossart, A., Sun, R., & Krapp, M. (2023). Conservation of heat and mass in P-SKRIPS version 1: the coupled atmosphere–ice–ocean model of the Ross Sea. *Geoscientific Model Development, 16(11), 3355–3373*. [https://doi.org/10.5194/gmd-16-3355-](https://doi.org/10.5194/gmd-16-3355-2023)
- 385 2023
- Manabe, S., & Stouffer, R. J. 1999. The role of thermohaline circulation in climate. *Tellus B, 51(1), 91–109*. <https://doi.org/10.1034/j.1600-0889.1999.00008.x>
- Morales Maqueda, M. A., A. J. Willmott, & N. R. T. Biggs 2004, Polynya dynamics: A review of observations and modeling, *Rev. Geophys., 42, RG1004*, doi:10.1029/2002RG000116.
- 390 Mathiot, P., Jourdain, N. C., Barnier, B., Gallée, H., Molines, J. M., Le Sommer, J., & Penduff, T. (2012). Sensitivity of coastal polynyas and high-salinity shelf water production in the Ross Sea, Antarctica, to the atmospheric forcing. *Ocean Dynamics, 62, 701–723*

- Miller, U. K., Zappa, C. J., Gordon, A. L., Yoon, S., Stevens, C., & Lee, W. S. (2024). High Salinity Shelf Water production rates in Terra Nova Bay, Ross Sea from high-resolution salinity observations. *Nature Communications*, 15(1). <https://doi.org/10.1038/s41467-023-43880-1>
- Moctezuma-Flores, M., Parmiggiani, F., Fragiaco, C., & Guerrieri, L. (2017). Synthetic aperture radar analysis of floating ice at Terra Nova Bay—an application to ice eddy parameter extraction. <https://www.semanticscholar.org/paper/Synthetic-aperture-radar-analysis-of-floating-ice-Moctezuma-Flores-Parmiggiani/5e0aba1638f19af80636249805558bf1d2ba9746>
- 395 Nicholls, K. W. (1997). Predicted reduction in basal melt rates of an Antarctic ice shelf in a warmer climate. *Nature*, 388(6641), 460–462. <https://doi.org/10.1038/41302>
- Orsi, A., Johnson, G., & Bullister, J. 1999. Circulation, mixing, and production of Antarctic Bottom Water. *Progress in Oceanography*, 43(1), 400 55–109. [https://doi.org/10.1016/s0079-6611\(99\)00004-x](https://doi.org/10.1016/s0079-6611(99)00004-x)
- Rusciano, E., Budillon, G., Fusco, G., & Spezie, G. 2013. Evidence of atmosphere–sea ice–ocean coupling in the Terra Nova Bay polynya (Ross Sea—Antarctica). *Continental Shelf Research*, 61–62, 112–124. <https://doi.org/10.1016/j.csr.2013.04.002>
- Savidge, E., Snow, T., Siegfried, M. R., Zheng, Y., Bôas, A. B. V., Bortolotto, G. A., Boehme, L., & Alley, K. E. (2023). Wintertime Polynya structure and variability from thermal remote sensing and Seal-Borne observations at Pine Island Glacier, West Antarctica. *IEEE Transactions on Geoscience and Remote Sensing*, 61, 1–13. <https://doi.org/10.1109/tgrs.2023.3271453>
- 405 Craig Stevens, Won Sang Lee, Giannetta Fusco, Sukyoung Yun, Brett Grant, Natalie Robinson & Chung Yeon Hwang (2017). The influence of the Drygalski Ice Tongue on the local ocean, *Annals of Glaciology*, 58(74), pp. 51–59. doi:10.1017/aog.2017.4
- Stevens, C., Yoon, S., Zappa, C. J., Miller, U. K., Wang, X., Elliott, F., Cornelissen, L., Lee, C., Yun, S., & Lee, W. S. 2024. Ocean processes south of the Drygalski Ice Tongue, western Ross Sea. *Deep Sea Research Part II Topical Studies in Oceanography*, 217, 105411. <https://doi.org/10.1016/j.dsr2.2024.105411>
- 410 Tamura, T., K. I. Ohshima, A. D. Fraser & G. D. Williams 2016, Sea ice production variability in Antarctic coastal polynyas, *J. Geophys. Res. Oceans*, 121, 2967–2979, doi:10.1002/2015JC011537.
- Uchida, H., Kawano, T., & Fukasawa, M. (2008). In situ calibration of moored CTDs used for monitoring abyssal water. *Journal of Atmospheric and Oceanic Technology*, 25(9), 1695–1702. <https://doi.org/10.1175/2008jtecho581.1>
- 415 Wang, Y., Zhou, M., Zhang, Z., & Dinniman, M. S. (2023). Seasonal variations in Circumpolar Deep Water intrusions into the Ross Sea continental shelf. *Frontiers in Marine Science*, 10. <https://doi.org/10.3389/fmars.2023.1020791>
- Williams, G. D., Bindoff, N. L., Marsland, S. J., & Rintoul, S. R. (2008). Formation and export of dense shelf water from the Adélie Depression, East Antarctica. *Journal of Geophysical Research Atmospheres*, 113(C4). <https://doi.org/10.1029/2007jc004346>
- Wong, A. P. S., Gilson, J., & Cabanes, C. (2023). Argo salinity: bias and uncertainty evaluation. *Earth System Science Data*, 15(1), 383–393. <https://doi.org/10.5194/essd-15-383-2023>
- 420 Yoon, S., Lee, W. S., Stevens, C., Jendersie, S., Nam, S., Yun, S., Hwang, C. Y., Jang, G. I., & Lee, J. (2020). Variability in high-salinity shelf water production in the Terra Nova Bay polynya, Antarctica. *Ocean Science*, 16(2), 373–388. <https://doi.org/10.5194/os-16-373-2020>
- Xu, Y., Zhang, W., Maksym, T., Ji, R., & Li, Y. (2023). Stratification Breakdown in Antarctic Coastal Polynyas. Part II: Influence of an ice tongue and coastline geometry. *Journal of Physical Oceanography*, 53(9), 2069–2088. <https://doi.org/10.1175/jpo-d-22-0219.1>
- 425 Otago Sea Ice Monitoring Station, <https://seaice.otago.ac.nz/trackers/overview/>
- MORSea: Marine Observatory in the Ross Sea, 2009. Italian National Antarctic Research Program (PNRA), coordinated by University of Naples “Parthenope” and CNR. <https://morsea.uniparthenope.it>
- Argo Fleet Monitoring - Euro-Argo. (n.d.-b) <https://fleetmonitoring.euro-argo.eu/dashboard?Status=Active,Inactive&WMO=3902666,5907101,6903812,6903795>

- 430 Nortek, Norway <https://www.nortekgroup.com/products/aquadopp2-6000-m/pdf>
Sea-Bird Scientific, Bellevue, WA, USA https://www.comm-tec.com/prods/mfgs/SBE/manuals_pdf/SBE37SM_016.pdf
Sea-Bird Scientific (n.d.). Frequently asked questions: CTD accuracy and effect of fouling/contamination on conductivity/salinity data. Sea-Bird Scientific Blog / Service Deployment FAQs. Available at: <https://blog.seabird.com/faqs/> (accessed 9/1/2026).
Sea-Bird Electronics. (2010). Application Note 31: Temperature and conductivity corrections (February 2010). Sea-Bird Electronics.
435 <https://imos.org.au/wp-content/uploads/2024/07/appnote31Feb10TempandCondCorrections.pdf>
Sea-Bird Scientific, Bellevue, WA, USA https://www.comm-tec.com/Prods/mfgs/SBE/brochures_pdf/56brochureApr11.pdf
Xylem. Inc., Rye Brook, NY, USA <https://epic.awi.de/id/eprint/45145/1/RCM9.pdf>